Rovibrational states of the H_2O–H_2 complex: An *ab initio* calculation

Ad van der Avoird[1,a] and David J. Nesbitt[2]
[1]*Theoretical Chemistry, Institute for Molecules and Materials, Radboud University Nijmegen, Heyendaalseweg 135, 6525 AJ Nijmegen, The Netherlands*
[2]*JILA, University of Colorado and National Institute of Standards and Technology and Department of Chemistry and Biochemistry, University of Colorado, Boulder, Colorado 80309-0440, USA*

(Received 3 November 2010; accepted 10 December 2010; published online 28 January 2011)

All bound rovibrational levels of the H_2O–H_2 dimer are calculated for total angular momentum $J = 0$–5 on two recent intermolecular potential surfaces reported by Valiron *et al.* [J. Chem. Phys. **129**, 134306 (2008)] and Hodges *et al.* [J. Chem. Phys. **120**, 710 (2004)] obtained through *ab initio* calculations. The method used handles correctly the large amplitude internal motions in this complex; it involves a discrete variable representation of the intermolecular distance coordinate R and a basis of coupled free rotor wave functions for the hindered internal rotations and the overall rotation of the dimer. The basis is adapted to the permutation symmetry associated with the para/ortho (p/o) nature of both H_2O and H_2 as well as to inversion symmetry. Dimers containing oH_2 are more strongly bound than dimers with pH_2, as expected, with dissociation energies D_0 of 33.57, 36.63, 53.60, and 59.04 $cm^{-1}$for pH_2O–pH_2, oH_2O–pH_2, pH_2O–oH_2, and oH_2O–oH_2, respectively, on the potential of Valiron *et al.* that corresponds to a binding energy D_e of 235.14 cm^{-1}. Rovibrational wave functions are computed as well and the nature of the bound states in the four different dimer species is discussed. Converged rovibrational levels on both potentials agree well with the high-resolution spectrum reported by Weida and Nesbitt [J. Chem. Phys. **110**, 156 (1999)]; the hindered internal rotor model that was used to interpret this spectrum is qualitatively correct. © *2011 American Institute of Physics*. [doi:10.1063/1.3533232]

I. INTRODUCTION

Collisions between water, H_2O, which is a predominant molecular species in interstellar clouds, and H_2, the most abundant molecule in the universe, play a critical role in important astrophysical phenomena.[1–4] One such phenomenon, for example, involves the formation of the so-called H_2O masers, whereby the combination of long path lengths and inverted H_2O internal state distributions in regions of star formation yields intense, amplified spontaneous emission on rotational lines of H_2O.[5,6] How such highly nonequilibrium rotational distributions of H_2O are formed is still not clear, but one putative mechanism is that this internal excitation is formed by collisions of hot H_2 gas outflows in star formation regions with H_2O in the interstellar medium.[3] Essential to any first principles understanding of such maser formation processes will clearly be a detailed knowledge of the underlying bimolecular collision dynamics, which in turn requires a rigorously accurate understanding of the H_2O–H_2 intermolecular potential.[2,7,8]

A second example from astrophysics is the recombination of H atoms to form H_2 on icy interstellar dust grains.[2,7] This represents a critical step in balancing photofragmentation with molecule reformation in the interstellar medium, which requires an understanding of the large amplitude quantum mechanics of how the newly formed H_2 interacts with and ultimately dissociates from the H_2O ice surface itself. Indeed, the dynamics of such H_2–H_2O ice grain species represents internally excited, quasibound levels of the weakly bound H_2O–H_2 complex. This highlights another key area in which a quantitatively benchmarked intermolecular potential for H_2O–H_2 plays a critically important role.

As yet another example of terrestrial as well as interstellar relevance, there have been some recent measurements by Dick *et al.* on the temperature collisional broadening[9] of the rotational lines of H_2O by H_2.[4,10] These studies exploit high resolution millimeter wave absorption spectroscopy of H_2O in a cold H_2 gas chamber, where the accessible temperatures range from 20 to 200 K. By detailed least squares fits of these THz transitions to a pressure broadened line shape, they infer the quantum state resolved pressure broadening coefficient for collisions of H_2O with He and H_2 as a function of temperature. The broadening coefficients with He exhibit only a simple and modest dependence on temperature. However, the trend for collisions of H_2O with H_2 as the colliding gas is qualitatively different: it exhibits an inverse power law rise for T_{cell} from 200 K down to 50 K, followed by an entirely unexpected, precipitous drop in the broadening rate below 50 K, with this behavior reiterated in all six rotational transitions studied. These results are currently somewhat controversial,[11,12] but if they are borne out by further experimental confirmation, this would be strong indication of novel collisional dynamics between H_2O and H_2 at low temperatures. This speaks to the importance of having high quality *ab initio* potential surfaces for H_2O–H_2 collisional interactions, which in turn must be rigorously tested by benchmarking against accurate experimental data. Specifically, the thrust of this paper is to facilitate a direct

[a]Electronic mail: A.vanderAvoird@theochem.ru.nl.

comparison of fully converged energy levels from quantum dynamical calculations on high quality *ab initio* potential surfaces against the known energy level structure obtained from high resolution spectroscopy of the weakly bound H_2O–H_2 complex.

Though there is much in the interstellar medium to motivate exploration into such fascinating collisional energy transfer dynamical phenomena, the H_2O–H_2 complex is both interesting and challenging in its own right in our world of chemical physics. For example, the quantum dynamics of large amplitude rearrangement of nuclei within the three atom (e.g., O + H_2) and four atom (e.g., H + H_2O) systems have only recently become possible in full dimensionality. However, this first required multiple years of efforts to (i) calculate high quality *ab initio* potential surfaces, (ii) find suitably efficient analytical representations of these potentials as well as (iii) develop sufficiently powerful quantum mechanical tools for accurately predicting energy level structures and large amplitude motion in such quantum states. Critical to this process has been the availability of high quality experimental data for rigorously testing the accuracy of such predicted surfaces, for example, from cluster, crossed molecular beam, photofragmentation, or photodetachment studies.

One important step up in complexity arises from the intermolecular dynamics of 5 atom systems (e.g., four H atoms + one heavy O atom), which currently represent a state-of-the-art frontier for both theory and experiment. As a case of particular relevance to interstellar chemistry, we tackle the weakly bound 5 atom H_2O–H_2 complex. Even under reduced dimensionality constraints associated with the covalently intact HOH and HH bonds, this is a challenging problem, requiring both (i) a high quality *ab initio* potential energy surface as well as (ii) the tools for extraction of quantum state energy levels on such a surface. Crucial to this work, therefore, has been the *ab initio* computation of interaction energies by a number of groups, which provide a first glimpse of the weakly bonded interaction.[13–15] Specifically, there are multiple global and local minima, one corresponding to a hydrogen-bonded structure with the H_2 being called the "proton donor" (in which the H_2 axis points along the C_{2v} axis of H_2O) as well as two "proton acceptor" sites (at which a OH points into the H_2 bond). Of special relevance to the calculations in this paper has been the recent development of a high level *ab initio* surface by Valiron *et al.*,[16] which maps out the potential in full dimensionality (9D) as a function of all internal degrees of freedom. Furthermore, this 9D potential has been suitably averaged over quantum motion associated with the high frequency stretching and bending degrees of freedom, yielding a high quality 5D potential energy surface explicitly tailored to a given intramolecular $H_2O(v_1, v_2, v_3)$ and $H_2(v)$ vibrational state. This potential has already been used in classical and quantum scattering calculations of rotationally and vibrationally inelastic H_2O–H_2 collision cross sections[17–21] and collisional line broadening.[22] In conjunction with sophisticated large basis set variational methods designed for obtaining quantum energy levels of weakly bound complexes, it permits us to obtain detailed predictions of intermolecular rovibrational energy levels for H_2O–H_2. Finally, these results in turn can be compared with previous experimental results from Weida and Nesbitt on rovibrationally resolved diode laser spectroscopy of this weakly bound complex in the HOH bending region.[23]

The first complete 5D potential for H_2O–H_2 computed in 1992 by Zhang *et al.*[15] turned out to be not so accurate by comparison with potential reported by Valiron *et al.*[16] The potential computed in 2004 by Hodges *et al.*[24] with rigid monomers in their vibrationally averaged geometries rather closely resembles the 5D ground state vibrationally averaged potential reported by Valiron *et al.* We found it worthwhile to compute the rovibrational energy levels of the complex also on the potential reported by Hodges *et al.*

The organization of this paper is as follows. Section II outlines the computational method, the two potential surfaces used, and the symmetry properties applied to simplify the calculations and in the comparison of the results with the experimental data. In Sec. III, we present and discuss our results and compare them with the high-resolution spectroscopic data by Weida and Nesbitt.[23] Section IV summarizes our conclusions.

II. COMPUTATIONAL METHOD, POTENTIAL SURFACE, AND SYMMETRY

A. Method

The method used in the calculation of the rovibrational levels of H_2O–H_2 is similar to the method developed for the water dimer; it is described in detail in Ref. 25. It starts from the Hamiltonian of a rotating dimer consisting of two rigid monomers, expressed in body-fixed (BF) dimer coordinates,[26]

$$H = T_A + T_B + \frac{1}{2\mu_{AB}R^2} \times \left[-\hbar^2 \frac{\partial}{\partial R} R^2 \frac{\partial}{\partial R} + J^2 + j_{AB}^2 - 2\mathbf{j}_{AB}\cdot\mathbf{J}\right] + V(R, \beta_A, \gamma_A, \beta_B, \alpha). \quad (1)$$

The H_2O and H_2 monomers are labeled A and B, respectively. The BF frame has its z-axis along the vector $\mathbf{R}$ that points from the center of mass of A to that of B. The coordinate R is the length of this vector and (Θ, Φ) are the polar angles of $\mathbf{R}$ with respect to a space-fixed (SF) frame. The Euler angles $\omega_A \equiv (\alpha_A, \beta_A, \gamma_A)$ define the orientation of H_2O with respect to the BF frame, $\omega_B \equiv (\beta_B, \alpha_B)$ are the polar angles of the H_2 axis relative to this frame. The planar reference geometry with angles $\omega_A = (0, 0, 0)$ and $\omega_B = (0, 0)$ is shown in Fig. 1(a); it lies in the xz-plane. This structure corresponds to the global minimum in the potential surface used, see Sec. II B. The potential $V(R, \beta_A, \gamma_A, \beta_B, \alpha)$ depends on the dihedral angle $\alpha = \alpha_B - \alpha_A$, while (Φ, Θ, α_A) are the overall rotation angles of the complex.

The operator $\mathbf{J}$ represents the total angular momentum, $\mathbf{j}_{AB} = \mathbf{j}_A + \mathbf{j}_B$ is the sum of the monomer angular momenta, and $\mu_{AB} = m_{H_2O}m_{H_2}/(m_{H_2O} + m_{H_2})$ is the dimer reduced mass. The components of the angular momentum operators in Eq. (1) are defined relative to the BF frame. The monomer kinetic energy operators for H_2O and H_2 are given by

$$T_A = A_x \left(j_{Ax}^{MF}\right)^2 + A_y \left(j_{Ay}^{MF}\right)^2 + A_z \left(j_{Az}^{MF}\right)^2 \quad (2)$$

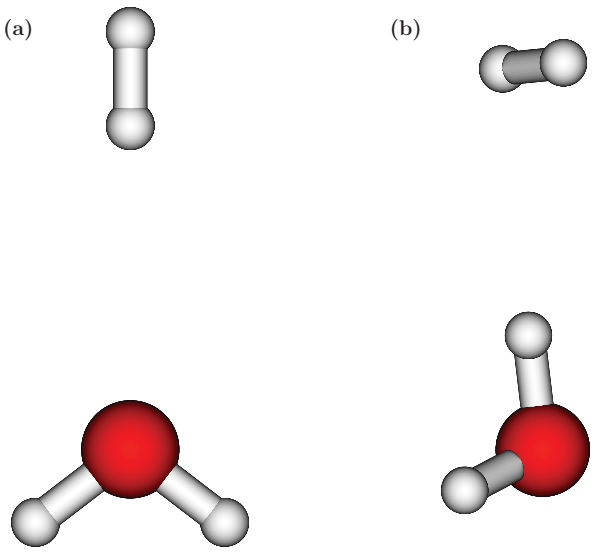

FIG. 1. (a) Planar equilibrium geometry of H_2O–H_2 with C_{2v} symmetry. Distance between the centers of mass $R_e = 5.82\,a_0$, binding energy $D_e = 235.14\ \mathrm{cm}^{-1}$. (b) Metastable structure of H_2O-H_2 with $\beta_A = 119°$, $\gamma_A = 0°$, $\beta_B = 90°$, $\alpha = 90°$, $R_e = 6.07\,a_0$, and $D_e = 199.40\ \mathrm{cm}^{-1}$.

and

$$T_B = B j_B^2. \tag{3}$$

The parameters A_x, A_y, A_z are the rotational constants of H_2O and B is the rotational constant of H_2. The superscript MF (molecule-fixed) implies that x, y, and z refer to the components of $\mathbf{j}_A$ along the principal axes of the H_2O monomer. We use the ground state experimental values for the rotational constants, i.e., $A_x = A_0 = 27.8806\ \mathrm{cm}^{-1}$, $A_y = C_0 = 9.2778\ \mathrm{cm}^{-1}$, and $A_z = B_0 = 14.5216\ \mathrm{cm}^{-1}$ for H_2O (Ref. 27) and $B = B_0 = 59.3398\ \mathrm{cm}^{-1}$ for H_2.[28] The atomic masses are 1.007 825 u for H and 15.994 915 u for O.

The basis in which the eigenstates of the Hamiltonian are computed is

$$\begin{aligned}|n, j_A, k_A, j_B, j_{AB}, K; J, M\rangle &= \chi_n(R)\left[\frac{(2j_A+1)(2j_B+1)(2J+1)}{128\pi^4}\right]^{1/2} \\ &\times \sum_{m_A m_B} D^{(j_A)}_{m_A k_A}(\omega_A)^* C_{j_B m_B}(\omega_B) \\ &\times \langle j_A m_A; j_B m_B | j_{AB} K\rangle\ D^{(J)}_{MK}(\Phi, \Theta, 0)^*. \end{aligned} \tag{4}$$

The radial basis functions $\chi_n(R)$ are computed by a sinc function discrete variable representation (DVR) (Refs. 29 and 30) on an equidistant grid of 96 points in the range from $R = 4$ to $26\,a_0$. At first, a one-dimensional radial Schrödinger equation was solved with a potential $V_0(R)$ that is a cut of the full five-dimensional potential surface through the minimum at angles $(\beta_A, \gamma_A, \beta_B, \alpha) = (0, 0, 0, 0)$. This potential has only four bound states, however, and we need a complete set of radial basis functions, so we constructed an alternative radial potential

$$V_{\mathrm{eff}}(R) = V_0(R) + \zeta R \tag{5}$$

by adding a linear potential with slope ζ. The choice of the parameter ζ was guided by minimizing the energy of the lower rovibrational states in full five-dimensional calculations with the lowest ten eigenfunctions $\chi_n(R)$ of the radial Hamiltonian with the potential $V_{\mathrm{eff}}(R)$. The selected value is $\zeta = 10^{-4}$ atomic units $= 21.947\ \mathrm{cm}^{-1}/a_0$. In the final calculations we used 20 basis functions $\chi_n(R)$ obtained from the radial eigenvalue equation with this optimized parameter.

The angular basis functions are coupled products of symmetric rotor functions—Wigner functions $D^{(j)}_{mk}(\alpha, \beta, \gamma)^*$ (Ref. 31)—and (Racah normalized) spherical harmonics $C_{jm}(\beta, \alpha)$. It is the same as the basis used in earlier work on the NH_3 dimer,[32–34] the water dimer,[25,35–38] and the benzene dimer,[39] except for the replacement of the symmetric rotor functions by spherical harmonics for the H_2 monomer B. The expression $\langle j_A m_A; j_B m_B | j_{AB} K\rangle$ is a Clebsch–Gordan coupling coefficient.[31] The quantum numbers J and M are exact quantum numbers and are fixed.

The kinetic energy operator is diagonal in this basis, except for the monomer asymmetric rotor terms for H_2O, cf. Eq. (2), and the small off-diagonal Coriolis coupling terms in the operator $2\mathbf{j}_{AB} \cdot \mathbf{J}$, see Ref. 32. In contrast with some of the earlier work on the water dimer[25,35,36,38] these off-diagonal Coriolis coupling terms were explicitly included. This implies that the angular momentum projection K on the dimer axis $\mathbf{R}$ is not an exact quantum number.

The potential is expanded in the same type of angular functions as used in the basis in Eq. (4). Since the potential is invariant under overall rotation only functions with $J = 0$ are needed to expand it. The potential is written as

$$V(R, \omega_A, \omega_B) = \sum_{L_A K_A L_B L} v_{L_A K_A L_B L}(R)\ A_{L_A K_A L_B L}(\omega_A, \omega_B) \tag{6}$$

with expansion functions

$$\begin{aligned}A_{L_A K_A L_B L}(\omega_A, \omega_B) &= (-1)^{L_A+L_B+L} \sum_{M_A M_B} \begin{pmatrix} L_A & L_B & L \\ M_A & M_B & 0 \end{pmatrix} \\ &\times D^{(L_A)}_{M_A K_A}(\omega_A)^* C_{L_B M_B}(\omega_B) \end{aligned} \tag{7}$$

and coefficients

$$\begin{aligned}v_{L_A K_A L_B L}(R) &= \frac{(2L_A+1)(2L_B+1)(2L+1)}{16\pi^2} \\ &\times \langle A_{L_A K_A L_B L}(\omega_A, \omega_B) | V(R, \omega_A, \omega_B)\rangle. \end{aligned} \tag{8}$$

With this expansion all angular matrix elements of the potential over the basis in Eq. (4) can be expressed in terms of 3-j and 9-j symbols.[25]

Tests of the convergence of the bound energy levels in full 5D calculations showed that the increase of $j_{A_{\max}}$ from 8 to 10 and of $j_{B_{\max}}$ from 6 to 8 lowers the bound energy levels by about 10^{-7} to $10^{-5}\ \mathrm{cm}^{-1}$. The levels of dimers with oH_2O and oH_2 are the most sensitive, which is not surprising since they require basis functions with odd k_A and j_B that are effectively truncated at maximum values of 7 and 5 when $j_{A_{\max}} = 8$ and $j_{B_{\max}} = 6$, for instance. In the final calculations we chose $j_{A_{\max}} = 10$ for H_2O and $j_{B_{\max}} = 8$ for H_2. The error introduced by using a contracted radial basis of 15 functions $\chi_n(R)$

instead of the full DVR grid was found to be about 10^{-4} cm^{-1}; in the final calculations we included 20 contracted radial basis functions. The radial grid had to be extended to the rather large R value of 26 a_0 in order to also converge bound states close to the dissociation limit. The dimension of the Hamiltonian matrices with the symmetry-adapted basis for $0 \leq J \leq 5$ ranges from about 20 000 to more than 160 000. The lowest 20 eigenvalues and eigenvectors of these matrices were obtained by means of the iterative algorithm of Davidson.[40]

B. Potential surface

A potential surface that includes all nine internal degrees of freedom of H_2O–H_2 was calculated *ab initio* by Valiron *et al.*[16] with the use of the CCSD(T)-R12 method (coupled-cluster with singles, doubles, and perturbative triples, explicitly correlated). In the same paper they also presented a 5D potential surface that includes only the five intermolecular degrees of freedom. The 5D potential was obtained by averaging the 9D potential over the ground state vibrational wave functions of H_2O and H_2. The global minimum in this potential corresponds to the planar geometry depicted in Fig. 1(a). According to Ref. 16 a local minimum occurs for the non-planar geometry shown in Fig. 1(b). Both of these geometries may be considered as hydrogen bonded: in Fig. 1(a) the H_2 monomer is the donor and H_2O the acceptor and in Fig. 1(b) H_2O is the donor and H_2 the acceptor.

Figure 2 shows a two-dimensional cut of the 5D potential for planar geometries as a function of the orientations of the H_2O symmetry axis and the H_2 bond axis. At each angular point the energy was minimized by optimizing R. This cut passes through the global minimum. Starting from the global minimum in Fig. 1(a) there is a narrow valley that slowly rises toward a planar geometry which resembles the local minimum in Fig. 1(b), except that the dihedral angle $\alpha = 0$, whereas it is 90° at the local minimum. As one will see below, the bound state wave functions tend to follow this valley, even though the intermolecular zero point vibrational energy is so high that they become strongly delocalized.

Valiron *et al.*[16] expressed their 5D potential in the form of an expansion,

$$V(R,\theta,\phi,\theta',\phi') = \sum_{l_1 m_1 l_2 l} v_{l_1 m_1 l_2 l}(R)\bar{t}_{l_1 m_1 l_2 l}(\theta,\phi,\theta',\phi'). \quad (9)$$

The expansion functions are

$$\bar{t}_{l_1 m_1 l_2 l}(\theta,\phi,\theta',\phi') = \alpha_{l_1 m_1 l_2 l}(1+\delta_{m_1 0})^{-1} \sum_{r_1 r_2} \begin{pmatrix} l_1 & l_2 & l \\ r_1 & r_2 & r \end{pmatrix} Y_{l_2 r_2}(\theta',\phi')\, Y_{l r}(\theta,\phi) \times \left[\delta_{m_1 r_1} + (-1)^{l_1+m_1+l_2+l}\delta_{-m_1 r_1}\right] \quad (10)$$

with the normalization factor

$$\alpha_{l_1 m_1 l_2 l} = \left[2(1+\delta_{m_1 0})^{-1}(2l_1+1)^{-1}\right]^{-1/2} \quad (11)$$

and $m_1 \geq 0$. Their coordinates are defined relative to a frame fixed to the H_2O monomer with the origin at the H_2O center of mass, the z-axis along the twofold symmetry axis with O at positive z, and the molecule lying in the xz-plane. The coordinates (θ,ϕ) are the polar angles of the intermolecular vector $\mathbf{R}$ and (θ',ϕ') are the polar angles of the H_2 axis. The coefficients in the expansion of Eq. (9) were obtained by least squares fitting to a number of *ab initio* calculated interaction energies. They were cubic spline interpolated as functions of R from $R = 3$ to 15 a_0 and extrapolated to a larger R with the correct asymptotic R^{-n} behavior.[16] Only 149 expansion coefficients $v_{l_1 m_1 l_2 l}(R)$ were needed to produce an accurate representation of the potential.

The angular coordinates of the potential in Eqs. (9) and (10) are different from the angular coordinates that describe the orientations of the monomers in our BF frame. In our BF

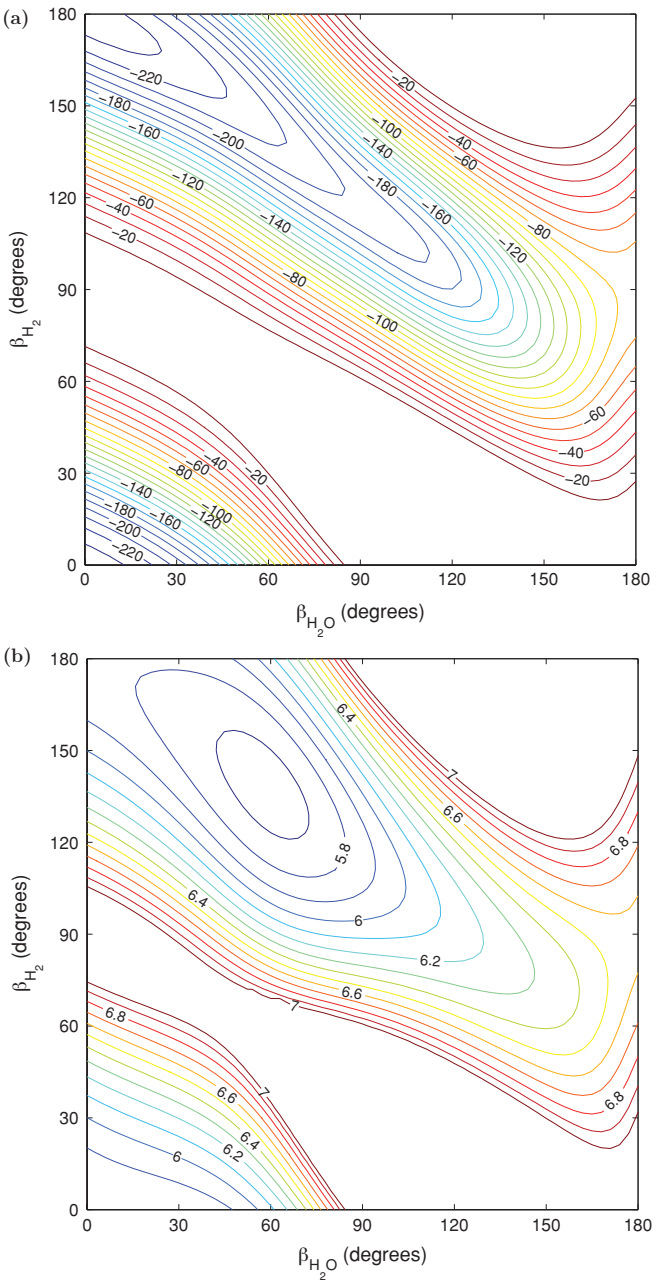

FIG. 2. (a) Cut of the 5D potential surface (in cm^{-1}) for planar geometries ($\gamma_A = 0$ and $\alpha = 0$) and R optimized to find the energy minimum for all angles. Panel (b) shows the optimized values of R (in a_0).

frame the orientation of the H_2O monomer is given by the Euler angles $(\alpha_A, \beta_A, \gamma_A)$ and the inverse Euler rotation over these angles rotates it back to the orientation that it has in the H_2O fixed frame of Valiron *et al.* It follows easily that the polar angles (θ, ϕ) of $\mathbf{R}$ in the latter frame are equal to the angles $(-\beta_A, -\gamma_A)$ or, equivalently, $(\beta_A, \pi - \gamma_A)$ in our BF frame. With the explicit use of the inverse Euler rotation matrix also the angles (θ', ϕ') can be expressed in terms of our Euler angles $(\alpha_A, \beta_A, \gamma_A)$ and (α_B, β_B). Then, the potential can be calculated in terms of our angular coordinates.

It is also possible, however, to derive directly the relation between the expansion functions in Eq. (10) and those in Eq. (7). We show this by starting with the expansion functions in general SF coordinates, see Ref. 32,

$$A_{L_A K_A L_B L}\left(\omega_A^{\mathrm{SF}}, \omega_B^{\mathrm{SF}}, \Theta, \Phi\right) = (-1)^{L_A+L_B+L} \sum_{M_A M_B M} \begin{pmatrix} L_A & L_B & L \\ M_A & M_B & M \end{pmatrix} \times D^{(L_A)}_{M_A K_A}\left(\omega_A^{\mathrm{SF}}\right)^{\star} C_{L_B M_B}\left(\omega_B^{\mathrm{SF}}\right) C_{LM}(\Theta, \Phi). \quad (12)$$

The angles ω_A^{SF} and ω_B^{SF} define the orientations of the monomers with respect to the SF frame. The potential is a scalar function and, hence, the expansion functions are coupled to a scalar. In other words, as written above, we use coupled angular basis functions with $J = 0$ in the expansion of the potential. Therefore, any frame rotation leaves the form of the expansion functions unaltered and the functions in different frames are simply obtained by substitution of the angular coordinates for each frame. In our BF frame the monomer angles are $(\omega_A, \omega_B) \equiv (\omega_A^{\mathrm{BF}}, \omega_B^{\mathrm{BF}})$ and the polar angles (Θ, Φ) of the vector $\mathbf{R}$ are $(0, 0)$. Use of the relation $C_{LM}(0, 0) = \delta_{M0}$ produces the expansion functions of Eq. (7). In the H_2O fixed frame the angles ω_A are $(0, 0, 0)$, the angles ω_B are (θ', ϕ'), and the polar angles (Θ, Φ) of $\mathbf{R}$ were called (θ, ϕ). Then one can use that $D^{(L_A)}_{M_A K_A}(0, 0, 0) = \delta_{M_A K_A}$, which yields the expansion functions in the H_2O fixed frame

$$(-1)^{L_A+L_B+L} \sum_{M_B M} \begin{pmatrix} L_A & L_B & L \\ K_A & M_B & M \end{pmatrix} C_{L_B M_B}(\theta', \phi')\, C_{LM}(\theta, \phi). \quad (13)$$

Comparing this with Eq. (10) and taking into account the different normalizations of the spherical harmonics C_{lm} and Y_{lm}, one finds the relation between our expansion coefficients in Eq. (6) and those in Eq. (9) that define the potential of Valiron *et al.*,

$$v_{L_A K_A L_B L}(R) = \begin{cases} (-1)^{l_1+l_2+l} f_{l_1 m_1 l_2 l}\, v_{l_1 m_1 l_2 l}(R), & \text{for } K_A \geq 0 \\ (-1)^{m_1} f_{l_1 m_1 l_2 l}\, v_{l_1 -m_1 l_2 l}(R), & \text{for } K_A < 0 \end{cases} \quad (14)$$

with factors

$$f_{l_1 m_1 l_2 l} = \frac{[(2l_1+1)(2l_2+1)(2l+1)(1+\delta_{m_1 0})/2]^{1/2}}{4\pi} \quad (15)$$

and $L_A = l_1$, $K_A = \pm m_1$, $L_B = l_2$, $L = l$.

Another potential for H_2O–H_2 that includes all five intermolecular degrees of freedom was calculated by Hodges *et al.*[24] with the use of scaled perturbation theory. This potential is not very different from the 5D ground state averaged potential of Valiron *et al.* It also has a global and a local minimum for dimer structures similar to those in Figs. 1(a) and 1(b). The binding energy D_e is slightly larger, 241.18 cm^{-1} at $R_e = 5.77\, a_0$ against 235.14 cm^{-1} at $R_e = 5.82\, a_0$ for the potential of Valiron *et al.*, while the depth of the local minimum is 214.48 cm^{-1} at $R = 5.96\, a_0$ and $\beta_A = 117^\circ$ instead of 199.40 cm^{-1} at $R = 6.07\, a_0$ and $\beta_A = 119^\circ$.

Before we can use this potential to calculate the rovibrational states of H_2O–H_2, it must be transformed to center-of-mass coordinates—Hodges *et al.* placed the H_2O origin on the O atom—and expanded according to Eq. (6). The angular integrals in the expansion coefficients given by Eq. (8) were evaluated numerically for each value of R by Gauss–Legendre quadrature for the angles β_A, β_B and Gauss–Chebysev quadrature for the angles γ_A, α. All expansion coefficients $v_{L_A K_A L_B L}(R)$ up to maximum L_A, L_B values of 12, 6 and $L = 18$ were included. The quadrature grid contained 13 points for β_A, 7 points for β_B, and 26 points for γ_A and for α. This expansion of the potential of Hodges *et al.* represents it around the global and local minima with an accuracy better than 0.01 cm^{-1}, in the long range the relative accuracy is even better, and in the repulsive region at $R = 4.5\, a_0$ the expansion differs from the original potential by about 1%. Most of the results in Sec. III were obtained with the potential reported by Valiron *et al.* because we believe its quality is somewhat higher; some results obtained with the potential reported by Hodges *et al.* are given for comparison.

C. Symmetry

The permutation–inversion (PI) or molecular symmetry group[41] of the H_2O–H_2 dimer with rigid monomers is isomorphic with the point group D_{2h} and may be denoted as $G_8 \equiv D_{2h}(\mathrm{M})$. It is generated by the permutation P_{12} that interchanges the H nuclei in H_2O, the permutation P_{34} that interchanges the H nuclei in H_2, and inversion E^*. Inversion has the following effect on the basis defined in Eq. (4),

$$E^*|n, j_A, k_A, j_B, j_{AB}, K; J, M\rangle = (-1)^{j_A+j_B-j_{AB}+k_A+J}|n, j_A, -k_A, j_B, j_{AB}, -K; J, M\rangle. \quad (16)$$

Basis functions with even/odd values of k_A are even/odd under the permutation P_{12}, basis functions with even/odd values of j_B are even/odd under P_{34}. Irreducible representations (irreps) of G_8 that are even and odd under P_{34} are labeled A and B, respectively, and irreps that are even or odd under P_{12} get the subscript 1 or 2. The superscript $+/-$ denotes the even/odd parity under E^*. We adapted the basis to the irreps of G_8 and performed calculations for each irrep separately, which yields a substantial reduction of the computer time needed. Table I shows the relation between the G_8 irreps and the quantum numbers k_A, which determines the para/ortho (p/o) H_2O nature of the states, and j_B, which determines whether the states belong to para or ortho H_2. The corresponding nuclear spin statistical weights are also listed. In our analysis of the rovibrational states we found it

TABLE I. Irreducible representations of G_8, quantum numbers k_A and j_B relevant for symmetry, para/ortho (p/o) nature of the monomers in H_2O–H_2, and nuclear spin statistical weights.

irrep	k_A	H_2O	j_B	H_2	Weight
A_1^+	even	p	even	p	1
A_1^-	even	p	even	p	1
A_2^+	odd	o	even	p	3
A_2^-	odd	o	even	p	3
B_1^+	even	p	odd	o	3
B_1^-	even	p	odd	o	3
B_2^+	odd	o	odd	o	9
B_2^-	odd	o	odd	o	9

convenient to use the spectroscopic parity ϵ, which is related to the parity $p = \pm 1$ under E^* as $p = \epsilon(-1)^J$. We follow the convention to label states of even/odd spectroscopic parity by e/f.

The equilibrium structure of H_2O–H_2 has point group symmetry C_{2v}, see Fig. 1(a). The isomorphic PI group $G_4 \equiv C_{2v}(M)$ is generated by P_{12} and E^*. The twofold rotation C_2 in C_{2v} maps onto the permutation P_{12}, the reflection σ_v in the xz plane of the equilibrium geometry maps onto E^*, and the reflection $\sigma_v' \equiv \sigma_{yz}$ maps onto P_{12}^*. This implies that there are two equivalent global minima in the potential related by the permutation P_{34}. Level splittings by tunneling between the two minima are not experimentally observable, however, because the states with even j_B that are even under P_{34} belong to complexes with pH_2 monomers, while the states with odd j_B that are odd under P_{34} belong to complexes with oH_2 monomers. The oH_2–H_2 states with odd k_A basis functions starting from $j_A = 1, k_A = \pm 1$ may be considered as being excited in the H_2O hindered internal rotation or bend mode.

The local minimum structure of H_2O–H_2 has point group symmetry C_s, see Fig. 1(b), of order two. Hence, there are four equivalent local minima in the potential surface. The four equivalent local minimum structures are interchanged by P_{12} and P_{34}, the reflection σ in C_s corresponds to the operation P_{34}^* in the PI group G_8.

III. RESULTS, COMPARISON WITH EXPERIMENT

A. Energy levels

Tables II–V show the energy levels calculated for $J = 0$–5. They contain all bound levels for these values of J; blank entries in the tables imply that the corresponding states are not bound. Although K is not an exact quantum number one can see in these tables that many states can be labeled with specific (approximate) K values. States with $K = 0$, $K = 1$, and $K = 2$ are called Σ, Π, and Δ, respectively. Since we did not find any bound levels with K values higher than 2, we omitted basis functions with K higher than 3 from the calculations for $J = 4$ and 5. Tests for $J = 3$ in which we omitted the basis functions with $K = 3$ show that such a restriction of the basis causes negligibly small errors if the lowest K omitted from the basis exceeds the highest K value of the bound states by at least 2. The percentage of Σ, Π, or Δ character of a state was obtained by summation of the squared eigenvector components with a given K over all other basis set labels. In addition we extracted effective m_A and m_B values for each $K = m_A + m_B$ from the eigenvectors by transforming the coefficients of the coupled basis functions in Eq. (4) to an uncoupled product basis labeled by m_A and m_B.

TABLE II. Rovibrational levels of pH_2O–pH_2 (in cm^{-1}), dissociation limit 0, $D_0 = 33.57\ cm^{-1}$. All states have more than 99% Σ character. The parity e/f is the spectroscopic parity.

$\Sigma(K = 0)$						
parity	$J = 0$	$J = 1$	$J = 2$	$J = 3$	$J = 4$	$J = 5$
e	–33.5663	–32.1841	–29.4334	–25.3431	–19.9596	–13.3528
e	–2.0615	–1.3979	–0.1628			

In Table II one observes that only Σ states of spectroscopic parity e are bound for pH_2O–pH_2. The dissociation energy $D_0 = 33.57\ cm^{-1}$ is much smaller than the binding energy $D_e = 235.14\ cm^{-1}$. Thus, the zero-point energy due to the intermolecular vibrations is a large fraction of the binding energy. As one will see below, the corresponding ground state wave function is strongly delocalized. This is, of course, a consequence of the small mass and large rotational constant of H_2, but also the rotational constants of H_2O are relatively large compared to those of most molecules. Just one excited intermolecular vibrational state is bound for pH_2O–pH_2, although barely and only for $J \leq 2$. When looking at the wave functions, below, it becomes clear that it is the intermolecular stretch mode that is excited. The end-over-end rotational constant B of the complex that can be extracted from the ground state levels for $J = 0$–3 is $0.6923\ cm^{-1}$, see Table VI. The value of B for the excited state is much smaller. Obviously the excited state is much more diffuse, which is not surprising since it is stretch excited and close to dissociation.

For oH_2O–pH_2 more states are bound, see Table III, of both parities e and f. The ground state of this species has Σ character. Since oH_2O and pH_2O have different nuclear spin states and the monomer nuclear spins are conserved at the time scale of the experiment the ground state oH_2O–pH_2 dimer dissociates into oH_2O with $j_A = 1, k_A = \pm 1$ and energy $23.7994\ cm^{-1}$ and ground state pH_2. The corresponding dissociation energy D_0 is $36.63\ cm^{-1}$, slightly higher than for pH_2O–pH_2. The projection m_A of the monomer angular momentum j_A on the intermolecular axis **R** is (approximately) 0 and also the total angular momentum projection $K = m_A + m_B$ equals 0. About 6 cm^{-1} above the Σ ground state there is a Π state with $K = 1$. From the contributions m_A and m_B of the individual monomers to the $K = 1$ value we conclude that m_A is approximately 1 in this Π state, while m_B is nearly 0. This is naturally related to the $j_A = 1$ and $j_B = 0$ nature of the oH_2O and pH_2 monomers from which this dimer is formed. The Π levels occur in pairs, of e and f parities. In our calculations the parity splittings originate from off-diagonal Coriolis terms in the Hamiltonian that couple the $K = 1$ levels with $K = 0$ levels. If one considers the dimer as a (prolate) near-symmetric rigid rotor this splitting is the asymmetry doubling. One can see in Table III that K becomes more strongly mixed for some of the excited states.

TABLE III. Rovibrational levels of oH_2O–pH_2 (in cm^{-1}), dissociation limit 23.7994 cm^{-1}, and $D_0 = 36.63$ cm^{-1}. In parentheses the Σ or Π character; if not indicated it is higher than 99%.

$\Sigma(K=0)$										
parity	$J=0$	$J=1$		$J=2$		$J=3$		$J=4$		$J=5$	
e	–12.8342	–12.0554	(91%)	–10.2452	(81%)	–7.2284	(74%)	–2.9472	(69%)	2.5914	(65%)
e	21.9456	21.8911	(60%)	22.5298	(55%)	23.7161	(51%)				
f	15.6570	17.3393	(97%)	20.6180	(91%)						
$\Pi(K=1)$										
parity		$J=1$		$J=2$		$J=3$		$J=4$		$J=5$	
e		–5.4371	(91%)	–1.7436	(81%)	3.4203	(74%)	9.8971	(69%)	17.5393	(66%)
e		7.3546		10.1354		14.2761		19.7355			
e		23.6188	(62%)								
f		–6.0622		–3.3522		0.6738		5.9645		12.4420	
f		6.9922	(97%)	9.1140	(91%)	12.3878	(86%)	16.8523	(81%)	22.5087	(76%)
f		22.9665									

The amount of mixing depends on the occurrence of $K = 0$ and $K = 1$ levels near to each other.

The number of bound levels for pH_2O–oH_2 is about the same as for oH_2O–pH_2, cf. Tables IV and III. Again, the ground state has Σ character. The ground state pH_2O–oH_2 dimer dissociates into ground state ($j_A = 0$) pH_2O and oH_2 with $j_B = 1$, energy 118.6796 cm^{-1}, and its dissociation energy D_0 with respect to this asymptotic limit is 53.60 cm^{-1}. This value of D_0 is substantially higher than for oH_2O–pH_2 and pH_2O–pH_2. The lowest Π state is now about 15 cm^{-1} higher than the Σ ground state. All of this indicates that the H_2 monomer likes to align itself parallel to the intermolecular axis **R**, rather than perpendicular to it (as it is in the Π state) or in a near-spherically averaged orientation (as it is in the dimers with pH_2). This provides the most attractive configuration of the H_2O dipole and the (positive) H_2 quadrupole and yields the strongest hydrogen bond with H_2 as the donor and H_2O as the acceptor. The *e*–*f* parity splitting (asymmetry doubling) of all Π states in pH_2O–oH_2 is considerably smaller than in oH_2O–pH_2.

Table V shows that oH_2O–oH_2 has by far the largest number of bound states of all species. Also the dissociation energy D_0 of 59.04 cm^{-1} with respect to the asymptotic energy of 23.7994 + 118.6796 = 142.4790 cm^{-1} of ($j_A = 1, k_A = \pm 1$) oH_2O and ($j_B = 1$) oH_2 is the highest. This is, of course, related with the fact that both monomers in their ortho states with $j_A = 1$ and $j_B = 1$ can be aligned and adopt the most favorable structure. Also the occurrence of Δ states with $K = m_A + m_B = 2$ can thus be understood; we checked that these correspond to projection angular momenta $m_A = 1$ and $m_B = 1$ of both monomers. Another feature by which this species is different from all others is that the ground state has $\Pi(K = 1)$ rather than $\Sigma(K = 0)$ character. In this Π state it is the oH_2O monomer that has $m_A = 1$, while the oH_2 monomer has $m_B = 0$. Again, this can be understood by looking at the average orientations of oH_2O in its rotational state with $j_A = 1, |k_A| = 1, |m_A| = 1$ and of oH_2 in its rotational state with $j_B = 1, m_B = 0$. We already mentioned that the oH_2 monomer is mostly aligned along the bond axis **R** when $m_B = 0$. The orientation of the oH_2O monomer

TABLE IV. Rovibrational levels of pH_2O–oH_2 (in cm^{-1}), dissociation limit 118.6796 cm^{-1}, and $D_0 = 53.60$ cm^{-1}. In parentheses the Σ or Π character; if not indicated it is higher than 99%.

$\Sigma(K=0)$										
parity	$J=0$	$J=1$		$J=2$		$J=3$		$J=4$		$J=5$	
e	65.0833	66.4978		69.3176	(99%)	73.5235	(97%)	79.0850	(96%)	85.9577	(94%)
e	110.1147	111.0995	(99%)	112.9661	(95%)	115.4595	(84%)	118.3203	(72%)		
e	115.3347	116.6230	(96%)								
f	117.9550										
$\Pi(K=1)$										
parity		$J=1$		$J=2$		$J=3$		$J=4$		$J=5$	
e		80.3777		83.1115	(99%)	87.1880	(97%)	92.5775	(95%)	99.2384	(93%)
e		111.6557	(98%)	113.9738	(92%)	117.4065	(81%)				
e		117.8067	(97%)								
f		80.4185		83.2321		87.4239		92.9571		99.7776	
f		111.5848	(98%)	113.8156	(94%)	117.1048	(92%)				
f		117.5606	(91%)	118.6543	(72%)						

TABLE V. Rovibrational levels of oH_2O–oH_2 (in cm^{-1}), dissociation limit 142.4790 cm^{-1}, and $D_0 = 59.04$ cm^{-1}. In parentheses the Σ, Π, or Δ character; if not indicated it is higher than 99%.

$\Sigma(K=0)$										
parity	$J=0$	$J=1$		$J=2$		$J=3$		$J=4$		$J=5$	
e	93.8950	95.5183	(98%)	98.7206	(95%)	103.4183	(91%)	109.4759	(83%)	116.6567	(65%)
e	114.4237	115.6019	(98%)	117.9706	(95%)	121.5421	(91%)	126.3138	(87%)	132.2530	(84%)
e	137.6869	138.7024	(94%)	140.5341	(91%)						
e	141.1963	142.2179	(95%)								
f	98.5952	99.0473	(56%)	100.9904	(52%)	104.3059	(49%)[a]	108.9712	(48%)	114.9522	(47%)
f	122.7973	124.1109	(97%)	126.7074	(83%)	130.5620	(63%)	135.6276	(43%)	141.6444	(17%)[b]
f	129.3100	130.5609		133.0475	(97%)	136.7088	(94%)	141.2724	(86%)		
f	140.9848	141.8469	(92%)								

$\Pi(K=1)$									
parity	$J=1$		$J=2$		$J=3$		$J=4$		$J=5$	
e	83.4343	(98%)	85.8061	(95%)	89.3986	(91%)	94.2288	(87%)	100.2968	(84%)
e	100.2101		102.7943	(97%)	106.6991	(94%)	111.9808	(87%)	118.7763	(72%)
e	126.4860	(98%)	129.5227	(89%)	133.7155	(78%)	138.2653	(62%)		
e	134.8039	(93%)	136.0663	(85%)	138.2846	(78%)	142.0035	(71%)		
e	139.2761	(96%)	140.5045	(89%)	142.3795	(77%)				
f	83.6637		86.4672	(99%)	90.6518	(97%)	96.1914	(96%)	103.0494	(93%)
f	101.1095	(56%)	104.4018	(50%)	108.8434	(45%)[c]	114.3668	(40%)	120.9185	(36%)
f	126.3829	(97%)	129.2727	(85%)	133.4666	(74%)	138.7797	(63%)		
f	135.1471		136.9126	(97%)	139.4872	(91%)				
f	139.1112	(92%)	140.1035	(79%)	141.7550	(72%)				

$\Delta(K=2)$								
parity	$J=2$		$J=3$		$J=4$		$J=5$	
e	110.8898	(98%)	115.0583	(95%)	120.5295	(92%)	127.2321	(88%)
e	127.0808	(93%)	130.9751	(86%)	136.0087	(74%)	141.1748	(25%)[d]
e	142.2767	(86%)						
f	110.9238	(97%)	115.2160	(92%)	120.9540	(84%)	128.0912	(75%)
f	127.1051	(86%)	131.0660	(70%)	136.2688	(53%)		
f	142.2422	(86%)						

[a]For $J \geq 3$ this state gets dominant Π character: 50%, 51%, 52% for $J = 3, 4, 5$, respectively.
[b]For $J = 5$ this state gets dominant Π character: 51%.
[c]For $J \geq 3$ this state gets dominant Σ character: 48%, 46%, 43% for $J = 3, 4, 5$, respectively.
[d]For $J = 5$ this state gets dominant Π character: 57%.

is more difficult to visualize, but it is clear that the rotational angular momentum vector $\mathbf{j}_A$ of oH_2O with $j_A = 1, |k_A| = 1$ is nearly parallel to its C_2 symmetry axis. The vector $\mathbf{j}_A$, and therefore also the C_2 axis of H_2O, is best aligned with the BF z-axis $\mathbf{R}$ when $|m_A| = 1$. Hence, the rotational state of oH_2 with $j_A = 1, |k_A| = 1, |m_A| = 1$ provides the most favorable orientation for the oH_2O monomer to act as the acceptor in the hydrogen bond with (aligned) H_2. The lowest Σ state is higher than the ground Π state by about 10 cm^{-1} and the Δ state is higher by about 27 cm^{-1}. It is interesting that our conclusion that in oH_2O–oH_2 the Π state is the ground state and the lowest Σ state is higher in energy was already predicted from a simple model by Weida and Nesbitt.[23]

Table VI lists the rotational constants of H_2O–H_2 that can be extracted from the levels calculated for $J = 0$–3 by fitting them in the same way as the experimentally determined levels in Ref. 23. As a brief reminder of this analysis procedure, a single $\Sigma \leftarrow \Sigma$ band was observed and assigned to pH_2O–oH_2, whereas two bands out of the same lower state ($\Pi \leftarrow \Pi$ and $\Sigma \leftarrow \Pi$) were observed for the oH_2O–oH_2 species. The lack of experimental evidence for either oH_2O–pH_2 or pH_2O–pH_2 complexes with pH_2 was attributed to differential stabilization of the oH_2 versus pH_2 dimers, which from detailed balance considerations leads to exponentially different equilibrium constants at the low temperatures of a supersonic expansion. The 11 cm^{-1} proximity between the two upper states for the oH_2O–oH_2 species suggested the importance of significant Coriolis interactions. This was taken into account via a simple 2×2 Hamiltonian in the unperturbed Σ, Π state basis,

$$\mathbf{H} = \begin{pmatrix} E_\Sigma^{(J)} & \beta\sqrt{J(J+1)} \\ \beta\sqrt{J(J+1)} & E_\Pi^{(J)} \end{pmatrix}, \tag{17}$$

where $\beta\sqrt{J(J+1)}$ represents the rotationally induced coupling between a $\Sigma(K=0)$ and $\Pi(K=1)$ state. $E_\Sigma^{(J)}$ and $E_\Pi^{(J)}$ are each given by appropriate unperturbed rotational energy level expressions in $J(J+1)$, while E_Σ and E_Π are the level origins. Furthermore, as the predicted $\Sigma(K=0)$ and

TABLE VI. Rotational and distortion constants B and D, $\Pi - \Sigma$ energy gap, and Coriolis coupling constant β (in cm^{-1}) from fits to the energy levels for $J = 0$–3 (see text). For the dimers with oH_2O the lowest Σ and Π levels are fit simultaneously with the inclusion of Coriolis coupling.

		Valiron *et al.* potential				Hodges *et al.* potential			
		B	D	$E_\Pi - E_\Sigma$	β	B	D	$E_\Pi - E_\Sigma$	β
pH_2O–pH_2	Σ	0.6923	5.89×10^{-4}			0.7103	5.91×10^{-4}		
oH_2O–pH_2	Σ	0.6940				0.7170			
	Π	0.6719		6.12	1.349	0.6876		8.24	1.382
pH_2O–oH_2	Σ	0.7085	3.94×10^{-4}			0.7171	3.87×10^{-4}		
oH_2O–oH_2	Π	0.7024	2.31×10^{-4}			0.7156	1.80×10^{-4}		
	Σ	0.7013	10.36×10^{-4}	–10.93	1.156	0.7171	11.72×10^{-4}	–10.06	1.158

$\Pi(K = 1)$ energy gap is comparable for oH_2O–pH_2 and oH_2O–oH_2, we apply an identical Coriolis analysis to the theoretical predictions for both of these complexes, as summarized in Table VI. These fits to the theoretical data offer several interesting insights into the internal rotor dynamics. For example, the Coriolis coupling constants β obtained can be compared with predictions in the simple free rotor limit. In this limit the monomer angular momenta $j_A$and j_B, their projections m_A and m_B on the intermolecular axis **R**, and the projection k_A of j_A on the H_2O monomer z-axis are good quantum numbers. Let us remind the reader that $K = m_A + m_B$. The Coriolis coupling term $-2(\mathbf{j}_A + \mathbf{j}_B) \cdot \mathbf{J}/(2\mu_{AB}R^2)$ in the Hamiltonian of Eq. (1) couples the $\Sigma(K = 0)$ and $\Pi(K = 1)$ levels through the shift operators,

$$\frac{-j_{A\pm}J_{\pm} - j_{B\pm}J_{\pm}}{2\mu_{AB}R^2}. \tag{18}$$

The first term shifts m_A and K by ± 1 and yields coupling matrix elements

$$-\left\langle \chi_{n'}(R) \left| \frac{1}{2\mu_{AB}R^2} \right| \chi_n(R) \right\rangle \times \sqrt{j_A(j_A+1) - m_A(m_A \pm 1)}\sqrt{J(J+1) - K(K \pm 1)} \tag{19}$$

between primitive uncoupled dimer basis functions with $j'_A = j_A$, $k'_A = k_A$, $j'_B = j_B$, $m'_A = m_A \pm 1$, $m'_B = m_B$, and $K' = K \pm 1$. Similarly, the second term shifts m_B and K. In the free internal rotor limit the radial and angular motions are decoupled, the R-dependent factor in the Coriolis coupling operator can be averaged over the radial wave function, and the radial matrix element in Eq. (19) can be replaced by the end-over-end rotational constant of the dimer $B = \langle 1/(2\mu_{AB}R^2)\rangle$.

As discussed above, the ground $\Sigma(K = 0)$ state of oH_2O–pH_2 is dominated by internal rotor basis functions with $j_A = 1$, $k_A = \pm 1$, $m_A = 0$, and $j_B = m_B = 0$. The lowest $\Pi(K = 1)$ state has similar approximate quantum numbers, except for m_A and K which are ± 1. Substition of these values into Eq. (19) shows that, in the free internal rotor limit, the coupling matrix element between normalized parity-adapted wave functions of the Σ and Π states becomes $-2B\sqrt{J(J+1)}$, i.e., the Coriolis coupling constant equals $2B$. The values of B for oH_2O–pH_2 are about 0.68 cm^{-1}, which yields $2B = 1.36$ cm^{-1}. The Coriolis coupling constant β of 1.35 cm^{-1} from the combined fit of the Σ and Π levels calculated for $J = 0$–3 is very close to this value. So me may conclude that oH_2O–pH_2 dimers behave close to the free internal rotor limit. It should be mentioned, however, that the error of the fit is relatively large in this case.

For oH_2O–oH_2 the approximate internal rotor quantum numbers of the ground $\Pi(K = 1)$ state are $j_A = 1$, $k_A = \pm 1$, $m_A = \pm 1$, $j_B = 1$, and $m_B = 0$. The approximate quantum numbers of the lowest Σ state are similar, except that $m_A = K = 0$. The free internal rotor limit with these values of the quantum numbers again yields a Coriolis coupling constant of $2B$. The value of B is about 0.70 cm^{-1} in this case, which gives $2B = 1.40$ cm^{-1}, while the fit of the calculated dimer levels yields a Coriolis coupling constant β of 1.16 cm^{-1}. So, the actual value is nearly 20% smaller than the free internal rotor value, which indicates that the internal rotations in oH_2O–oH_2 are more strongly hindered than in oH_2O–pH_2.

The energy levels calculated with the potential of Hodges *et al.* are similar to those in Tables II–V. The wells in this potential are slightly deeper than in the potential of Valiron *et al.* and the rovibrational states are slightly lower in energy. This is reflected by the dissociation energies D_0, which are 36.11 cm^{-1} for pH_2O–pH_2, 40.43 cm^{-1} for oH_2O–pH_2, 57.07 cm^{-1} for pH_2O–oH_2, and 62.71 cm^{-1} for oH_2O–oH_2, i.e., about 7% higher than with the potential of Valiron *et al.* For some of the higher states with energies not far below the dissociation limit this implies that they remain bound up to a higher J value than the levels in Tables II–V. Furthermore, it implies that there exists a (barely) bound $\Delta(K = 2)$ state also for pH_2O–oH_2. The end-over-end rotational constants B are slightly larger than with the potential of Valiron *et al.*, see Table VI, in accordance with the somewhat smaller equilibrium distance R_e in the potential of Hodges *et al.*

B. Wave functions

The character of the various bound states of the different nuclear spin species can be determined by looking at their wave functions. Wave function plots also give insight in the nature of the excited intermolecular vibrations. The ground state $J = 0$ wave function of pH_2O–pH_2 plotted as a function of R at the equilibrium angles $\omega_A = (0, 0, 0)$ and $\omega_B = (0, 0)$ has a maximum near $R = 6.3\,a_0$. Angular plots

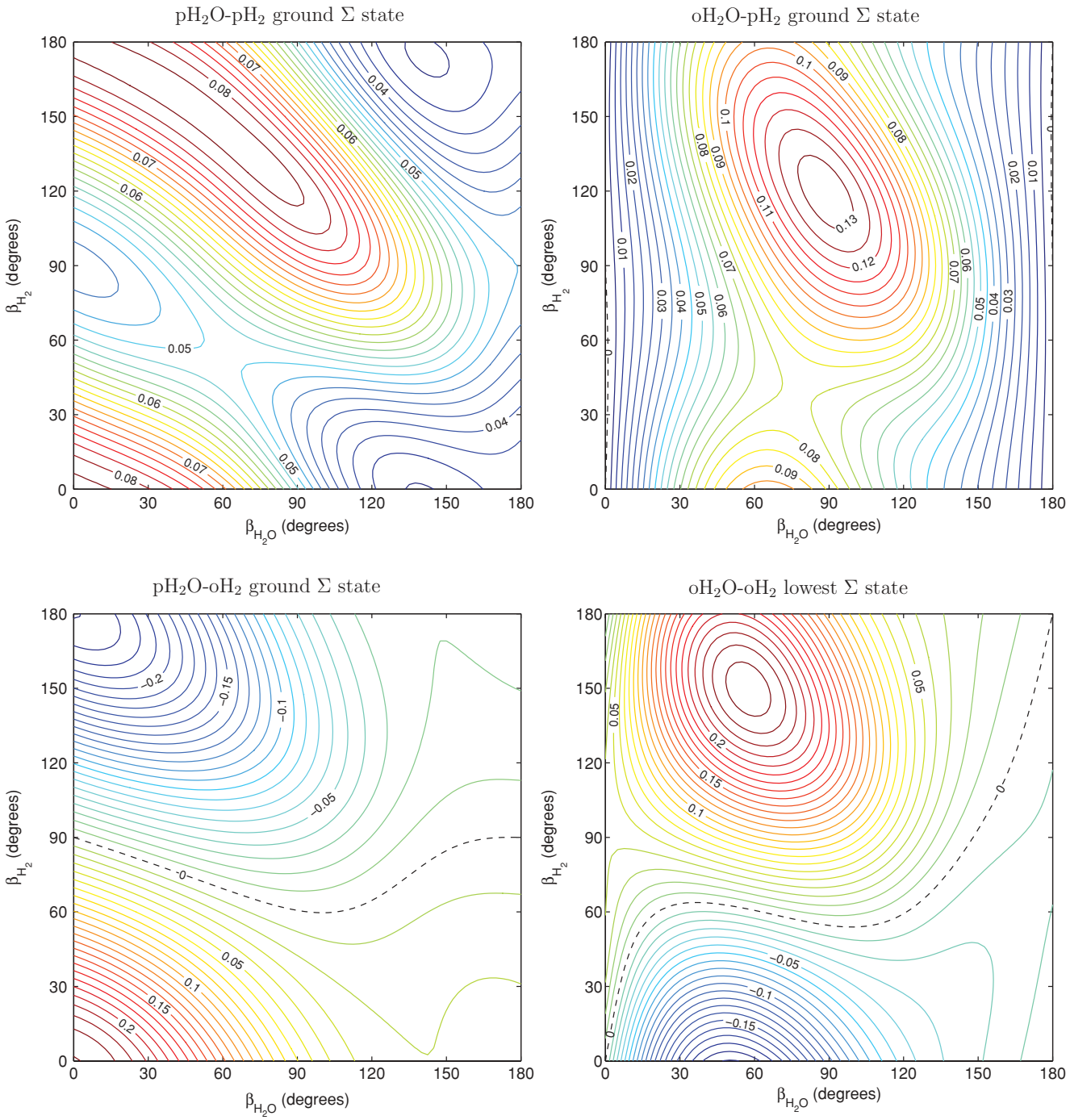

FIG. 3. Wave functions for $J = 0$, planar geometries, $R = 6.30\,a_0$.

of the $J = 0$ wave functions at this R value for planar geometries are shown in Fig. 3. In these angular plots one can nicely see the different characteristics of the wave functions for para/ortho H_2O and para/ortho H_2 monomers. All these wave functions are for $J = 0$, so they all belong to Σ states with $K = 0$. The ground state wave function of pH_2O–pH_2 does not have any nodes. It is strongly delocalized, but still one can see clearly that it has its largest amplitude in the valley of the potential surface, cf. Fig. 2, that gradually rises from the global minimum in the direction of the local minimum. For oH_2O–pH_2 the wave function contains only functions with odd k_A and must have nodes at $\beta_A = 0^\circ$ and 180°. This restriction on the wave function pushes its maximum away from $\beta_A = 0^\circ$ to a point further up into the potential valley. The wave function of pH_2O–oH_2 contains only functions with odd j_B and must change sign between $\beta_B = 0^\circ$ and 180°. For $\beta_A = 0^\circ$ and 180° this implies that this wave function must have a node at $\beta_B = 90^\circ$, as one can see. In Fig. 3 one can also see that this symmetry restriction tends to push the wave function of pH_2O–oH_2 away from the higher part of the potential valley toward the global minimum. The wave function of oH_2O–oH_2 must both have a node at $\beta_A = 0^\circ$ and 180° and change sign between $\beta_B = 0^\circ$ and 180°. In the corresponding panel of Fig. 3 this is clearly visible.

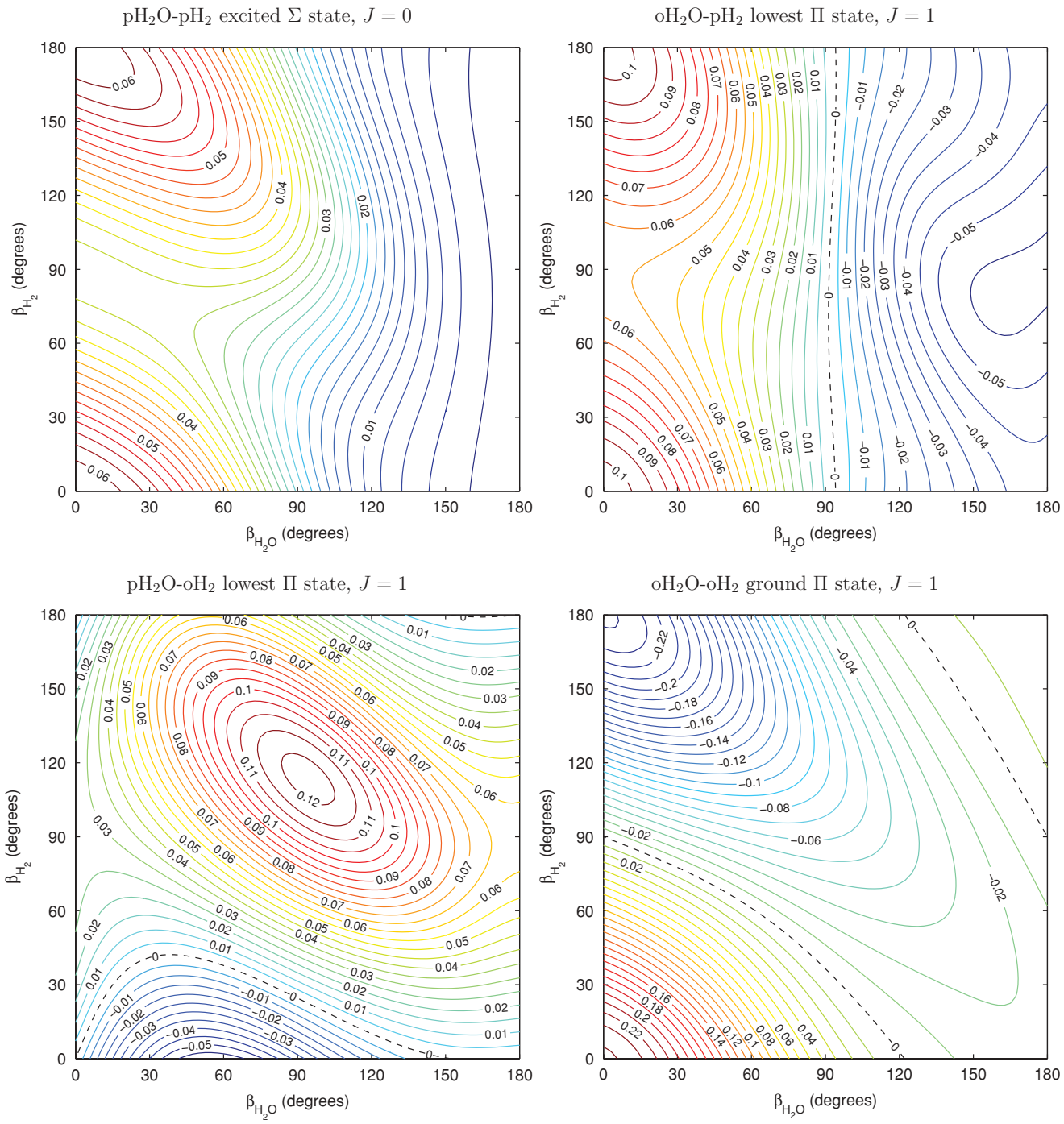

FIG. 4. Wave functions for $J = 0$ and 1, planar geometries, $R = 6.30\,a_0$.

A radial cut of the wave function of the second (barely) bound state of pH_2O–pH_2 for $J = 0$ shows that it has as a node in R, so this state is radially excited. This implies that the intermolecular stretch has a fundamental frequency of 31.5 cm^{-1}. The same holds for the lowest excited $J = 0$ parity e bound states of oH_2O–pH_2 and pH_2O–oH_2; the corresponding stretch frequencies are 34.8 and 45.0 cm^{-1}, respectively. The ratio of these three stretch frequencies is well in line with the dissociation energies D_0 of the three dimer species, which are 33.57, 36.63, and 53.60 cm^{-1}, in the same order. For oH_2O–oH_2 the situation is more complicated; all three excited states of parity e for $J = 0$ have a radial node. The second excited state seems to be mostly stretch excited, since it has considerable amplitude both inside and outside of the node. The first excited state has only little amplitude outside the radial node, and the third excited state has only small amplitude inside. If we consider the second excited state as the stretch fundamental the corresponding stretch frequency is 43.8 cm^{-1}, but it is clear that in oH_2O–oH_2 the radial excitations are more strongly mixed with excitations in the angular coordinates.

We saw in Tables II–V that H_2O–H_2 dimers except for pH_2O–pH_2 also have bound states of Π character, i.e., with approximately $K = 1$. For oH_2O–oH_2 the ground state is of Π type. Figure 4 shows the $J = 1$ wave functions of the

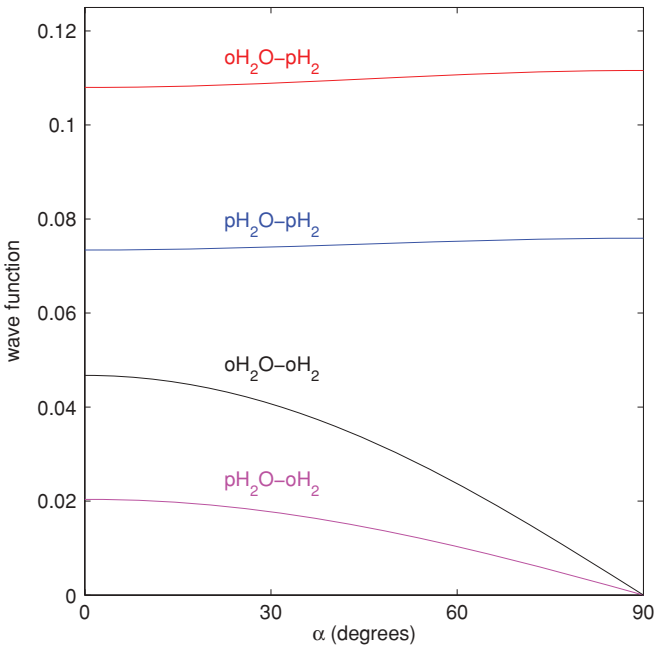

FIG. 5. Wave functions of lowest Σ states for $J = 0$, nonplanar geometries with $\beta_A = 119°$, $\gamma_A = 0°$, $\beta_B = 90°$, and $R = 6.30\,a_0$.

lowest Π states for the three nuclear spin species that possess bound Π states and the second $J = 0$ Σ state for pH_2O–pH_2. As discussed above, the latter is stretch excited and it is illustrated in the upper left panel of Fig. 4 that it does not have a node in the angular coordinates. There is some arbitrariness in the plots of $J = 1$ wave functions since they depend on the overall rotation angles (Φ, Θ, α_A). We chose $M = 0$ and $\Theta = 90°$, $\alpha_A = 0°$, since the real part of the overall rotation wave function with $(J, M, K) = (1, 0, 1)$ has its maximum amplitude at these angles and does not depend on Φ. The contour plots of the Π states in Fig. 4 show typical differences with the corresponding plots in Fig. 3 for the Σ states. One may notice, in particular, that the angles β_A or β_B where the nodal planes in the wave functions meet the edges of the contour plots are typically shifted by 90° for the Π states relative to the Σ states. Again, one may observe that the amount of localization of the wave functions and the geometries where they have their maximum amplitudes are determined to some extent by the nodal plane structure imposed by the symmetry. This illustrates that the change of the overall rotation quantum number K from 0 to 1 significantly affects the (hindered) internal rotations of the monomers.

In order to get an idea of the amplitude of the bound state wave functions in the region of the nonplanar metastable structure displayed in Fig. 1(b), we show plots (in Fig. 5) of the same wave functions as in Fig. 3 for geometries that start from a planar structure with the same coordinates $\beta_A = 119°$, $\gamma_A = 0°$, $\beta_B = 90°$ as the metastable geometry. The system is planar when $\alpha = 0°$ and arrives at the local minimum in the potential when $\alpha = 90°$. One observes that the wave functions of pH_2 complexes have considerable amplitude at the local minimum, slightly higher than at the corresponding planar structure and not much lower than the amplitude at their maximum, cf. Fig. 3. The amplitudes of the wave functions of oH_2 complexes are substantially smaller in this region due to the neighborhood of a nodal plane. One can see in Fig. 5 that this nodal plane actually passes through the local minimum at $\alpha = 90°$, as it must because of symmetry requirements. This does not imply, however, that the presence of a relatively deep local minimum is less important for the properties of the oH_2 complexes.

Wave functions of spectroscopic parity f have a nodal plane for planar geometries, including the equilibrium geometry. For this reason the f states with $K = 0$ may be considered as excited out-of-plane intermolecular vibrations, but it should be realized that they have rather low energies and look more like hindered rotations. As already mentioned, the e/f parity doublets for $K > 0$ are split by (off-diagonal) Coriolis coupling between the internal and overall rotations of the dimer but may also be considered as asymmetry doublets if we regard the dimer as a prolate near-symmetric rotor.

C. Comparison with experiment

A high resolution spectrum of the H_2O–H_2 complex was measured in the region of the ν_2 bend origin of H_2O at 1594.7 cm^{-1}.[23] In scans from 1582 to 1622 cm^{-1} three bands were observed which were all assigned to transitions in the two dimer species containing oH_2. The band between 1589 and 1603 cm^{-1} corresponds to $\Sigma \leftarrow \Sigma$ transitions in pH_2O–oH_2 and the band between 1590 and 1594 cm^{-1} corresponds to $\Pi \leftarrow \Pi$ transitions in oH_2O–oH_2. The end-over-end rotational and distortion constants extracted from the rotationally resolved band for pH_2O–oH_2 are $B = 0.7182$ cm^{-1}, $D = 3.57 \times 10^{-4}$ cm^{-1}, and $H = -8.9 \times 10^{-7}$ cm^{-1}. From a fit of the levels calculated for $J = 0$ to 5 we obtain $B = 0.7080$ cm^{-1}, $D = 3.75 \times 10^{-4}$ cm^{-1}, and $H = -10.4 \times 10^{-7}$ cm^{-1}, in very good agreement with the experimental data. The fact that even the distortion constants agree so well implies in particular that the long range part of the potential surface of Valiron *et al.* is accurate.

The band between 1590 and 1594 cm^{-1} assigned to the $\Pi \leftarrow \Pi$ transitions in oH_2O–oH_2 shows e/f parity splittings that are inconsistent with a semirigid rotor behavior of the complex. Hence, the transitions in this band were analyzed[23] with the aid of a model that includes the hindered internal rotations. In such a model the parity splittings between the Π levels of parity e/f are due to Coriolis coupling of the Π states to nearby Σ states, as in our calculations. Also $\Sigma \leftarrow \Pi$ transitions in combination with the ν_2 monomer transitions were predicted on the basis of this model and were actually found at frequencies between 1603 and 1622 cm^{-1}. An analysis of all the experimental data gave rotational constants B of 0.7055 and 0.7113 cm^{-1} for the Σ and Π states, respectively. From the same type of analysis of our levels calculated with the potential of Valiron *et al.* we obtain 0.7013 and 0.7024 cm^{-1}. The observed energy difference between the lowest Σ and Π energy levels in oH_2O–oH_2 is 10.55 cm^{-1}, while our calculations yield 10.93 cm^{-1}. Thus, our calculations not only reproduce the correct ordering of the Π and Σ states in oH_2O–oH_2 but also the energy gap between them is very realistic, which in turn depends sensitively on the anisotropy of the potential surface. Also the Coriolis coupling

constant of the Π and Σ levels could be extracted: the measured data yield 1.166 cm^{-1} and we calculated 1.156 cm^{-1}. A fit of the levels calculated with the potential of Hodges *et al.* gave rotational constants B of 0.7171 and 0.7156 cm^{-1} for the Σ and Π states, respectively, an energy gap of 10.06 cm^{-1} between those states, and a Coriolis coupling constant of 1.158 cm^{-1}. Obviously, the agreement between our calculations with both potentials and experiment is very good, which implies that both the potential surfaces of Valiron *et al.*[16] and of Hodges *et al.*[24] are accurate.

IV. CONCLUSIONS

This paper describes the calculation of the rovibrational states of the H_2O–H_2 dimer on two recently developed 5D intermolecular potential surfaces obtained through high level *ab initio* calculations. The variational method employed involves a discrete variable representation of the intermolecular distance R and a basis of coupled free rotor wave functions for the hindered internal rotations and the overall rotation of the dimer. The basis is adapted to the permutation symmetry associated with the para/ortho (p/o) nature of both H_2O and H_2 as well as to inversion symmetry. All bound rovibrational levels of the four different nuclear spin species: pH_2O–pH_2, oH_2O–pH_2, pH_2O–oH_2, and oH_2O–oH_2, are computed for both parities and $J = 0$–5.

We found that a large fraction of the binding energy D_e, which is 235.14 cm^{-1} in the potential of Valiron *et al.*,[16] goes into the intermolecular vibrational zero-point energy: the dissociation energies D_0 on this potential are only 33.57, 36.63, 53.60, and 59.04 cm^{-1} for pH_2O–pH_2, oH_2O–pH_2, pH_2O–oH_2, and oH_2O–oH_2, respectively. Wave functions, which are also calculated, show that the complex is very floppy and that the intermolecular vibrations are more like hindered internal rotations. Still, they show a marked preference of the system to explore the low energy region of the potential that extends from the hydrogen-bonded structure at the global minimum geometry, with the H_2 monomer as the donor and H_2O as the acceptor, to the only slightly less stable local minimum geometries, which are hydrogen-bonded with H_2O as the donor and with H_2 as the acceptor. The observation that ortho monomers lead to stronger binding than para monomers is not surprising, but in excellent confirmation of experiment.[23] Specifically, pH_2O and pH_2 can only orient themselves under the influence of the anisotropic interaction potential when their $j = 0$ ground states mix with excited rotational states. By way of contrast, however, both oH_2O and oH_2 have degenerate $j = 1$ ground states in which the monomers can be aligned even without any mixing. Especially for pH_2 with its large rotational constant of nearly 60 cm^{-1} and lowest excited state with $j = 2$, this leads to a much smaller value of D_0 than for oH_2. The ground state wave functions indeed show that the monomers want to orient themselves as much as they can for the given nuclear spin species, such that the dimer resembles the most stable hydrogen-bonded structure with C_{2v} symmetry. The wave functions have considerable amplitude also at the higher lying local minima, however.

All four species have a bound excited intermolecular stretch state, with fundamental frequencies that are not much lower than the dissociation energies. The species that include at least one ortho monomer also have excited hindered internal rotor states of different Σ, Π, and Δ character, i.e., with $K = 0$, 1, and 2. The ground state is Σ, except for oH_2O–oH_2 where it is of Π type. Also the greater stability of the Π state in oH_2O–oH_2 can be explained by considering the optimum orientations of the monomers, as discussed above.

The converged rovibrational levels can be compared with the high-resolution spectrum of the H_2O–H_2 dimer measured by Weida and Nesbitt.[23] Three bands were observed in this spectrum, in the range of the H_2O monomer bend mode; all transitions were assigned to pH_2O–oH_2 and oH_2O–oH_2. The data that could be extracted from the measured spectrum and compared with our calculated energy levels are the rotational and distortion constants of both species and, for oH_2O–oH_2, the energy gap between the Σ and Π states that are mixed by Coriolis coupling, as well as the coupling constant. We find good agreement with experiment for all of these data for the levels calculated on the potential of Valiron *et al.*,[16] which confirms that this potential is accurate. Also for the levels calculated on the somewhat older potential of Hodges *et al.*[24] we get good agreement, which is perhaps not so surprising since the two potentials are quite similar. The advantage of the potential of Valiron *et al.* is that it is 9D and includes also the coupling between the inter- and intramolecular degrees of freedom. The 5D potential that we used was obtained by averaging the 9D potential over the ground state vibrational wave functions of the H_2O and H_2 monomers. It can also be averaged over excited vibrational states of the monomers and can be used in calculations on dimers that are excited both in the intramolecular and intermolecular modes. Finally, we may conclude from our calculations that the hindered internal rotor model used by Weida and Nesbitt[23] to interpret their experimental spectrum, although simplified, is qualitatively correct.

ACKNOWLEDGMENTS

We thank Alexandre Faure and Laurent Wiesenfeld for making available the Fortran code of their potential. This work has been supported in part (D.J.N.) by funds from the National Science Foundation. We also would like to acknowledge additional assistance through the Senior Alexander von Humboldt Award program for providing the opportunity to work together. Finally, we note that while writing up this work we became aware of complementary efforts in the Carrington group to be published in this same issue. We would like to acknowledge Tucker Carrington and Xiaogang Wang for useful discussions.

[1] B. Rowland, M. Fisher, and J. P. Devlin, J. Chem. Phys. **95**, 1378 (1991).
[2] H. G. Hixson, M. J. Wojcik, M. S. Devlin, J. P. Devlin, and V. Buch, J. Chem. Phys. **97**, 753 (1992).
[3] T. R. Phillips and S. Green, Astrophys. Space Sci. **224**, 537 (1995).
[4] M. J. Dick, B. J. Drouin, and J. C. Pearson, Phys. Rev. A **81**, 022706 (2010).
[5] R. J. Cohen, Rep. Prog. Phys. **52**, 881 (1989).
[6] P. R. Rowland and R. J. Cohen, Mon. Not. R. Astr. Soc. **220**, 233 (1986).
[7] V. Buch and J. P. Devlin, J. Chem. Phys. **94**, 4091 (1991).
[8] V. Buch, J. Chem. Phys. **97**, 726 (1992).
[9] J. M. Dutta, C. R. Jones, T. M. Goyette, and F. C. Delucia, Icarus **102**, 232 (1993).

[10]M. J. Dick, B. J. Drouin, and J. C. Pearson, J. Quant. Spectrosc. Radiat. Transf. **110**, 619 (2009).
[11]A. F. Krupnov, Phys. Rev. A **82**, 036703 (2010).
[12]B. J. Drouin, J. C. Pearson, and M. J. Dick, Phys. Rev. A **82**, 036704 (2010).
[13]H. Lischka, Chem. Phys. **2**, 191 (1973).
[14]A. Moroz, R. L. Sweany, and S. L. Whittenburg, J. Phys. Chem. **94**, 1352 (1990).
[15]Q. Zhang, L. Chenyang, Y. Ma, F. Fish, M. M. Szczesniak, and V. Buch, J. Chem. Phys. **96**, 6039 (1992).
[16]P. Valiron, M. Wernli, A. Faure, L. Wiesenfeld, C. Rist, S. Kedzuch, and J. Noga, J. Chem. Phys. **129**, 134306 (2008).
[17]A. Faure, L. Wiesenfeld, M. Wernli, and P. Valiron, J. Chem. Phys. **123**, 104309 (2005).
[18]A. Faure, P. Valiron, M. Wernli, L. Wiesenfeld, C. Rist, J. Noga, and J. Tennyson, J. Chem. Phys. **122**, 221102 (2005).
[19]A. Faure, L. Wiesenfeld, M. Wernli, and P. Valiron, J. Chem. Phys. **124**, 214310 (2006).
[20]M.-L. Dubernet, F. Daniel, A. Grosjean, A. Faure, P. Valiron, M. Wernli, L. Wiesenfeld, C. Rist, J. Noga, and J. Tennyson, Astron. Astrophys. **460**, 323 (2006).
[21]A. Faure, N. Crimier, C. Ceccarelli, P. Valiron, L. Wiesenfeld, and M. L. Dubernet, Astron. Astrophys. **472**, 1029 (2007).
[22]L. Wiesenfeld and A. Faure, Phys. Rev. A **82**, 040702 (2010).
[23]M. J. Weida and D. J. Nesbitt, J. Chem. Phys. **110**, 156 (1999).
[24]M. P. Hodges, R. J. Wheatley, G. K. Schenter, and A. H. Harvey, J. Chem. Phys. **120**, 710 (2004).
[25]G. C. Groenenboom, P. E. S. Wormer, A. van der Avoird, E. M. Mas, R. Bukowski, and K. Szalewicz, J. Chem. Phys. **113**, 6702 (2000).
[26]G. Brocks, A. van der Avoird, B. T. Sutcliffe, and J. Tennyson, Mol. Phys. **50**, 1025 (1983).
[27]F. C. DeLucia, P. Helminger, R. L. Cook, and W. Gordy, Phys. Rev. A **5**, 487 (1972).
[28]G. Herzberg and L. L. Howe, Can. J. Phys. **37**, 636 (1959).
[29]D. T. Colbert and W. H. Miller, J. Chem. Phys. **96**, 1982 (1992).
[30]G. C. Groenenboom and D. T. Colbert, J. Chem. Phys. **99**, 9681 (1993).
[31]D. M. Brink and G. R. Satchler, *Angular Momentum*, 3rd ed. (Clarendon, Oxford, 1993).
[32]A. van der Avoird, P. E.S. Wormer, and R. Moszynski, Chem. Rev. **94**, 1931 (1994).
[33]J. W. I. van Bladel, A. van der Avoird, P. E. S. Wormer, and R. J. Saykally, J. Chem. Phys. **97**, 4750 (1992).
[34]E. H. T. Olthof, A. van der Avoird, and P. E. S. Wormer, J. Chem. Phys. **101**, 8430 (1994).
[35]R. Bukowski, K. Szalewicz, G. C. Groenenboom, and A. van der Avoird, Science **315**, 1249 (2007).
[36]R. Bukowski, K. Szalewicz, G. C. Groenenboom, and A. van der Avoird, J. Chem. Phys. **128**, 094314 (2008).
[37]W. Cencek, K. Szalewicz, C. Leforestier, R. van Harrevelt, and A. van der Avoird, Phys. Chem. Chem. Phys. **10**, 4716 (2008).
[38]X. Huang, B. J. Braams, J. M. Bowman, R. E. A. Kelly, J. Tennyson, G. C. Groenenboom, and A. van der Avoird, J. Chem. Phys. **128**, 034312 (2008).
[39]A. van der Avoird, R. Podeszwa, K. Szalewicz, C. Leforestier, R. van Harrevelt, P. R. Bunker, M. Schnell, G. von Helden, and G. Meijer, Phys. Chem. Chem. Phys. **12**, 8219 (2010).
[40]E. R. Davidson, J. Comput. Phys. **17**, 87 (1975).
[41]P. R. Bunker and P. Jensen, *Molecular Symmetry and Spectroscopy*, ed. (NRC Research Press, Ottawa, 1998).